Theory of high-harmonic generation with quantum light

Haoyu Liu [1], Hanxu Zhang [1], Xu Wang [1,*] and Jianmin Yuan [1,2,†]
[1]*Graduate School, China Academy of Engineering Physics, Beijing 100193, China*
[2]*Institute of Atomic and Molecular Physics, Jilin University, Changchun 130012, China*

(Received 16 September 2025; revised 14 November 2025; accepted 4 June 2026; published 22 June 2026)

High-harmonic generation (HHG) driven by intense quantum light has recently emerged as a new frontier in strong-field physics. Yet, the mechanism underlying HHG with nonclassical fields such as bright squeezed vacuum (BSV) light—characterized by a vanishing mean electric field—remains elusive. In this work, we develop a fully quantum theory for HHG under arbitrary quantum driving fields. We show that the fluctuation component of the dipole correlation operator plays a central role in HHG with quantum light and is essential for BSV-driven HHG. Furthermore, our framework reveals the photon statistics distribution within individual harmonics and across different harmonics, demonstrating that the statistics inherit the statistical properties of the driving field. This theory overcomes key limitations of existing approaches and uncovers new quantum features of HHG in the presence of nonclassical light.

DOI: 10.1103/y3gr-tsns

I. INTRODUCTION

High-harmonic generation (HHG) is a fundamental nonlinear process in intense laser-matter interactions [1–3], widely used to generate extreme-ultraviolet radiation and attosecond pulses [4–9]. It has been successfully described by classical and semiclassical models, such as the three-step model [10–12] and the strong-field approximation [13], where the laser field is treated classically.

Recent advances in producing intense squeezed light [14–22] have enabled the experimental realization of HHG with quantum light [23–25]. This development challenges classical-field-based interpretations, especially for bright squeezed vacuum (BSV) states, where the mean electric field vanishes. To address this regime, theoretical approaches based on the Husimi distribution [26–28] have been employed to represent quantum-light-driven HHG as a superposition of coherent-state (classical-field) responses [29–34]. These methods have also been extended to atomic single and double ionization under quantum driving fields [35–37]. Despite these advances, these methods remain semiclassical in nature: The spectra are obtained by averaging over a mixture of classical fields with varying intensities—particularly after discarding the off-diagonal terms of the Husimi distribution [31], which eliminates quantum coherences and thus prevents an accurate characterization of the driving field's photon statistics and squeezing properties [38]. Moreover, it remains unsettled whether the averaging should be performed incoherently [30,32] or coherently [29,33,34].

To overcome these limitations, we develop a fully quantum (FQ) theory that directly yields the quantum state of the harmonic modes under arbitrary quantum driving fields. It connects the HHG spectra and photon statistics of harmonic modes with the atomic dipole correlation operator. The use of dipole correlation function—originally introduced in quantum optics to define emission spectra of driven atomic systems [39–43] and formalized in the Scully-Lamb-Glauber model [39,40]—provides a natural foundation for this generalization. Our framework is nonrelativistic but includes effects of radiation reaction perturbatively [44,45]. We validate the framework by numerically solving the time-dependent Schrödinger equation for coupled atom-light systems driven by amplitude-squeezed coherent (ASC), phase-squeezed coherent (PSC), and BSV states. Our results demonstrate that the fluctuation component of the two-time dipole correlation operator is the key physical quantity governing HHG with quantum light, particularly for BSV driving. Moreover, the theory predicts the photon statistics distribution both within individual harmonics and across different harmonics, uncovering intrinsic quantum correlations in HHG that go beyond semiclassical descriptions.

II. METHODS

The Hamiltonian of the coupled quantum light-atom system is $\hat{H} = \hat{H}_{\rm A} + \hat{H}_{\rm F} + \hat{H}_{\rm int}$, where $\hat{H}_{\rm A}$ is the atomic Hamiltonian, $\hat{H}_{\rm F} = \sum_k \omega_k \hat{a}_k^\dagger \hat{a}_k$ is the Hamiltonian of the electromagnetic field, and $\hat{H}_{\rm int} = -\hat{\boldsymbol{d}} \cdot \hat{\boldsymbol{E}}$ describes atom-field interaction. The dipole operator is $\hat{\boldsymbol{d}} = \hat{d}\boldsymbol{\zeta}$ with orientation vector $\boldsymbol{\zeta}$, and the quantized electric field operator is $\hat{\boldsymbol{E}} = \sum_k \hat{\boldsymbol{E}}_k = i\sum_k \epsilon_k^{(1)}(\hat{a}_k - \hat{a}_k^\dagger)\boldsymbol{\epsilon}_k$, with $\boldsymbol{\epsilon}_k$ being the polarization vector and $\epsilon_k^{(1)} = \sqrt{\omega_k/2\epsilon_0 V}$ being the single-photon

*Contact author: xwang@gscaep.ac.cn
†Contact author: jmyuan@gscaep.ac.cn

field amplitude for mode $k \equiv \{\boldsymbol{k}, \sigma\}$ (V is the quantization volume, ϵ_0 is the vacuum permittivity, $\boldsymbol{k}$ is the wave vector, and σ is the polarization index). We use a one-dimensional model atom with $\hat{H}_\mathrm{A} = \hat{p}^2/2 - 1/\sqrt{\hat{x}^2 + \nu^2}$, where $\hat{x}$ and $\hat{p}$ are the position and momentum operators of the electron. The soft-core parameter [46] is set to $\nu^2 = 0.67$, giving a ground-state energy of -0.79 a.u., closely matching the ionization potential of a neon atom.

The total Hamiltonian $\hat{H}$ can be separated as $\hat{H} = \hat{H}_0 + \hat{V}$, where $\hat{H}_0 = \hat{H}_\mathrm{A} + \hat{H}_\mathrm{F} - \hat{\boldsymbol{d}} \cdot \hat{\boldsymbol{E}}_l$ includes the interaction between the atom and the single driving laser mode l and $\hat{V} = -\hat{\boldsymbol{d}} \cdot \sum_{q \neq l} \hat{\boldsymbol{E}}_q$ accounts for the coupling of the atom to all nondriving radiation modes. In the interaction picture with respect to $\hat{H}_0$, the perturbation operator is $\hat{V}_\mathrm{I}(t) = e^{i\hat{H}_0 t} \hat{V} e^{-i\hat{H}_0 t} = -\hat{\boldsymbol{d}}_\mathrm{I}(t) \cdot \sum_{q \neq l} \hat{\boldsymbol{E}}_q(t)$, where the field operator for mode q evolves as $\hat{\boldsymbol{E}}_q(t) = i\epsilon_q^{(1)}(\hat{a}_q e^{-i\omega_q t} - \hat{a}_q^\dagger e^{i\omega_q t})\boldsymbol{\varepsilon}_q$ and the dipole operator is given by $\hat{\boldsymbol{d}}_\mathrm{I}(t) = \hat{U}_l(t,0)\hat{\boldsymbol{d}}\hat{U}_l^\dagger(t,0)$. Here, $\hat{U}_l(t,0) = e^{i\hat{H}_l t}$ is the time-evolution operator associated only with the driving laser mode and $\hat{H}_l = \hat{H}_\mathrm{A} + \omega_l \hat{a}_l^\dagger \hat{a}_l - \hat{\boldsymbol{d}} \cdot \hat{\boldsymbol{E}}_l$. In this picture, the wavefunction of the system $|\Psi(t)\rangle_\mathrm{I}$ satisfies the time-dependent Schrödinger equation:

$$i\frac{\partial |\Psi(t)\rangle_\mathrm{I}}{\partial t} = \hat{V}_\mathrm{I}(t)|\Psi(t)\rangle_\mathrm{I}, \tag{1}$$

with the formal solution

$$|\Psi(t)\rangle_\mathrm{I} = \hat{T} e^{-i\int_0^t \hat{V}_\mathrm{I}(t_1)dt_1} |\Psi(0)\rangle_\mathrm{I}, \tag{2}$$

where $\hat{T}$ denotes the time-ordering operator. The initial state is taken as $|\Psi(0)\rangle_\mathrm{I} = |g, \phi_l, 0_q\rangle \equiv |g\rangle \otimes |\phi_l\rangle \otimes |0_{q\neq l}\rangle$, with $|g\rangle$ the atomic ground state, $|\phi_l\rangle$ the quantum state of the driving mode, and $|0_{q\neq l}\rangle$ the vacuum state of all nondriving radiation modes.

Because the radiation field is much weaker than the strong driving field, the interaction $\hat{V}_\mathrm{I}(t)$ can be treated perturbatively [47,48]. Retaining terms up to second order in the expansion ($\sim\mathcal{O}([\epsilon_q^{(1)}]^2)$), Eq. (2) reduces to

$$\begin{aligned}|\Psi(t)\rangle_\mathrm{I} \approx |g, \phi_l, 0_q\rangle &- \sum_{q\neq l} \epsilon_q^{(1)} \int_0^t dt_1 \hat{\boldsymbol{d}}_\mathrm{I}(t_1)\cdot\boldsymbol{\varepsilon}_q e^{i\omega_q t_1}|g, \phi_l, 1_q\rangle \\ &- \sum_{q\neq l} \left[\epsilon_q^{(1)}\right]^2 \hat{\mathcal{M}}(t, -\omega_q, \omega_q)|g, \phi_l, 0_q\rangle \\ &+ \sqrt{2}\sum_{q\neq l} \left[\epsilon_q^{(1)}\right]^2 \hat{\mathcal{M}}(t, \omega_q, \omega_q)|g, \phi_l, 2_q\rangle \\ &+ \sum_{q,p\neq l} \epsilon_q^{(1)}\epsilon_p^{(1)} \hat{\mathcal{M}}(t, \omega_q, \omega_p)|g, \phi_l, 1_q, 1_p\rangle, \end{aligned} \tag{3}$$

where $\hat{\mathcal{M}}(t, \pm\omega_m, \pm\omega_n) \equiv \int_0^t dt_1 \int_0^{t_1} dt_2 \hat{\boldsymbol{d}}_\mathrm{I}(t_1)\cdot\boldsymbol{\varepsilon}_m \hat{\boldsymbol{d}}_\mathrm{I}(t_2)\cdot\boldsymbol{\varepsilon}_n e^{\pm i\omega_m t_1} e^{\pm i\omega_n t_2}$. Equation (3) remains a formal solution because the dipole operator in the interaction picture already includes the coupling to the driving field. The corresponding Schrödinger-picture wavefunction is $|\Psi(t)\rangle = e^{-i\hat{H}_0 t}|\Psi(t)\rangle_\mathrm{I}$. The harmonic yield $Y(\omega_q)$ (photon number) at frequency ω_q along propagation direction $\boldsymbol{q}$, evaluated at the end of the driving pulse ($t = t_\mathrm{e}$), is given to leading order by

$$\begin{aligned} Y(\omega_q) &= \sum_\sigma \langle\Psi(t_\mathrm{e})|\hat{a}_q^\dagger \hat{a}_q|\Psi(t_\mathrm{e})\rangle \\ &= \left[\epsilon_q^{(1)}\right]^2 \int_0^{t_\mathrm{e}} dt_1 \int_0^{t_\mathrm{e}} dt_2 e^{-i\omega_q(t_2-t_1)} \\ &\quad\times \langle g, \phi_l|\hat{d}_\mathrm{I}(t_2)\hat{d}_\mathrm{I}(t_1)|g, \phi_l\rangle \sin^2\theta. \end{aligned} \tag{4}$$

Here, θ is the angle between the radiation mode propagation and the dipole direction. For simplicity, we set $\theta = 90^\circ$ (observation perpendicular to the dipole). Thus, the harmonic radiation is determined by the two-time correlation of the dipole operator.

We now move to the frequency domain and define the dipole operator $\hat{d}_\mathrm{I}(\omega) \equiv \int_0^{t_\mathrm{e}} dt e^{i\omega t}\hat{d}_\mathrm{I}(t)$. Using the operator fluctuation decomposition, $\hat{d}_\mathrm{I}(\omega) = \int_0^{t_\mathrm{e}} dt e^{i\omega t}[\langle\hat{d}_\mathrm{I}(t)\rangle\hat{I} + \Delta\hat{d}_\mathrm{I}(t)] \equiv \langle\hat{d}_\mathrm{I}(\omega)\rangle\hat{I} + \Delta\hat{d}_\mathrm{I}(\omega)$, with $\hat{I}$ denoting the identity operator, the harmonic yield becomes

$$\begin{aligned} Y(\omega_q) &= \left[\epsilon_q^{(1)}\right]^2 \langle g, \phi_l|\hat{d}_\mathrm{I}(\omega_q)^\dagger \hat{d}_\mathrm{I}(\omega_q)|g, \phi_l\rangle \\ &= \left[\epsilon_q^{(1)}\right]^2 [\langle\hat{d}_\mathrm{I}(\omega_q)\rangle^* \langle\hat{d}_\mathrm{I}(\omega_q)\rangle + \langle\Delta\hat{d}_\mathrm{I}(\omega_q)^\dagger \Delta\hat{d}_\mathrm{I}(\omega_q)\rangle], \end{aligned} \tag{5}$$

where the expectation value $\langle\cdots\rangle = \langle g, \phi_l|\cdots|g, \phi_l\rangle$. For coherent-state driving, the first term in the square brackets represents the spectral intensity from the dipole expectation value and gives the dominant HHG signal, as discussed further in Sec. IV C and Refs. [49,50]. For a BSV state, where the mean electric field is zero and thus $\langle\hat{d}_\mathrm{I}(t)\rangle$ and $\langle\hat{d}_\mathrm{I}(\omega)\rangle$ vanish, HHG originates entirely from dipole fluctuations. In practical calculations, we can insert into Eq. (5) a complete basis $\sum_{\xi,n}|\xi, n\rangle\langle\xi, n|$ of the coupled atom-field system ($|\xi\rangle$ denoting atomic states and $|n\rangle$ denoting field states):

$$Y(\omega_q) = \left[\epsilon_q^{(1)}\right]^2 \sum_{\xi,n} \langle g, \phi_l|\hat{d}_\mathrm{I}(\omega_q)^\dagger|\xi, n\rangle\langle\xi, n|\hat{d}_\mathrm{I}(\omega_q)|g, \phi_l\rangle. \tag{6}$$

In this work, we use the Fock-state basis for the radiation field. Introducing canonical operators of the light field, $\hat{y} = (\hat{a}_l^\dagger + \hat{a}_l)/\sqrt{2\omega_l}$ and $\hat{p}_y = i\sqrt{\omega_l/2}(\hat{a}_l^\dagger - \hat{a}_l)$, the Hamiltonian $\hat{H}_l$ becomes $\hat{H}_l = \hat{H}_\mathrm{A} + \hat{p}_y^2/2 + \omega_l\hat{y}^2/2 + \sqrt{2/\omega_l}\epsilon_l^{(1)}\hat{d}\hat{p}_y$, which facilitates efficient numerical propagation of the coupled state $e^{-i\hat{H}_l t}|g, \phi_l\rangle$ in a two-dimensional space [51–53]. The intensity of the driving laser is given by $I = c\omega_l N/V = \varepsilon_0 c|E|^2/2$, where c is the speed of light, N is the number of photons, and V is the quantization volume. The effective electric field is $|E| = \sqrt{2\omega_l N/\epsilon_0 V}$ [54,55]. The results depend primarily on $|E|$, i.e., on the ratio N/V, rather than on the absolute value of N. The convergence of this representation is discussed in Sec. IV D. Nonlinear atomic responses emerge once $|E|$ is sufficiently strong [56–58]. For a coherent state with parameter α, the photon number $N_\mathrm{coh} = |\alpha|^2$. For a BSV state, the photon number depends only on the squeezing parameter r: $N_\mathrm{squ} = \sinh^2 r$. For PSC or ASC states, the total photon number includes both components: $N = N_\mathrm{coh} + N_\mathrm{squ}$. A parameter $\chi = N_\mathrm{squ}/N_\mathrm{coh}$ can be introduced to characterize the relative contribution of squeezing.

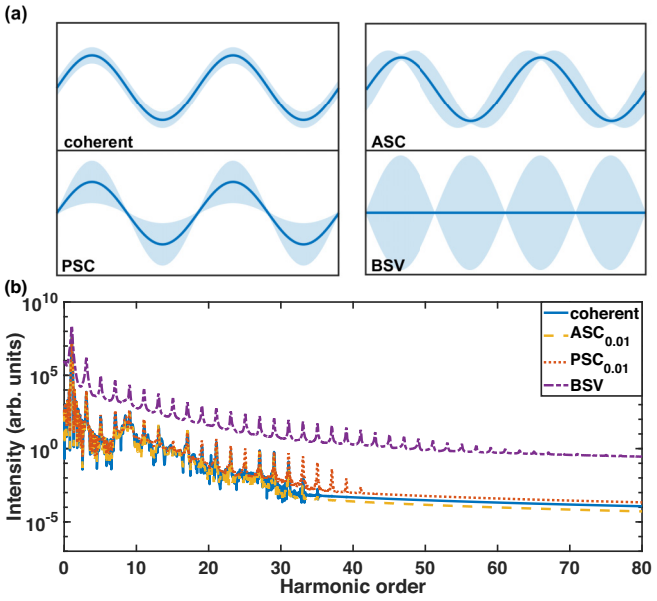

FIG. 1. (a) Schematic illustration of the field mean (solid line) and fluctuations (shaded area) for the coherent, ASC, PSC, and BSV states. (b) HHG spectra of a model Ne atom ($I_p = 0.79$ a.u.) obtained with our theory for coherent, BSV, and ASC/PSC light with $\chi = 0.01$. The driving laser has a wavelength of 800 nm, peak intensity 10^{14} W/cm^2, and duration of 15 cycles. All subsequent results use the same laser parameters.

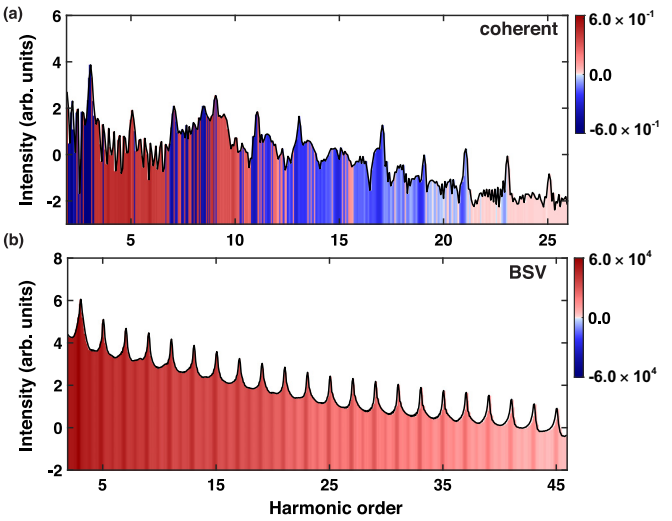

FIG. 2. Expectation value of the normally ordered variance of the number operator for each harmonic mode under (a) coherent light and (b) BSV light. Positive, negative, and zero values correspond to super-Poissonian, sub-Poissonian, and Poissonian statistics, respectively.

III. RESULTS

A. HHG with different quantum light states

Figure 1(a) schematically illustrates the mean field and quantum fluctuations of the driving states considered. Figure 1(b) shows the corresponding HHG spectra for a coherent state, a BSV state, and ASC/PSC states with $\chi = 0.01$. The BSV state produces a much broader spectrum (extending up to 65th harmonic) and an HHG yields several orders of magnitude higher than the other states. In contrast, the coherent and ASC/PSC states generate spectra of comparable amplitude, with PSC showing a slight extension and ASC a slight compression relative to the coherent case (up to 35th harmonic). These differences reflect the distinct fluctuation properties of the fields. BSV light exhibits much larger peak electric field fluctuations, which strongly enhance the nonlinear response. As a bunched light source [59], BSV further amplifies multiphoton channels, leading to both spectral extension and yield enhancement. PSC light inherits modestly larger peak-amplitude fluctuations than a coherent state, giving a weak BSV-like tendency, whereas ASC light shows suppressed peak-amplitude fluctuations and increased phase noise, which reduce HHG efficiency.

B. Quantum statistics of high harmonics

The second-order terms in Eq. (3) allow evaluation of quantum statistical properties of the high-harmonic modes. For a harmonic mode q, we compute the normally ordered variance of the number operator [60–62]:

$$\langle\Psi(t_e)| : (\Delta\hat{N}_q)^2 : |\Psi(t_e)\rangle = \langle\Psi(t_e)|\hat{a}_q^\dagger\hat{a}_q^\dagger\hat{a}_q\hat{a}_q|\Psi(t_e)\rangle - (\langle\Psi(t_e)|\hat{a}_q^\dagger\hat{a}_q|\Psi(t_e)\rangle)^2, \quad (7)$$

which is directly related to $\langle\hat{\mathcal{M}}^\dagger(t_e)\hat{\mathcal{M}}(t_e)\rangle$ through the second-order photon-emission amplitudes in Eq. (3). A positive value indicates super-Poissonian statistics, a negative value indicates sub-Poissonian statistics, and zero corresponds to Poissonian statistics.

Figure 2 presents the expectation values of this variance for coherent and BSV driving light. Under coherent light, the values fluctuate around zero, with slight positive or negative deviations. This indicates that high-harmonic generated by a coherent state remain essentially coherent, with only minor quantum corrections. In contrast, BSV driving light yields strictly positive values, markedly enhanced at harmonic peaks, clearly revealing super-Poissonian statistics. These results demonstrate that the quantum statistical properties of the driving light are imprinted onto the generated harmonics.

In addition, we calculate cross-correlation functions to characterize the statistical relations between two harmonic modes q and p [60–64]:

$$C_{qp} = \langle\Psi(t_e)|\hat{a}_q^\dagger\hat{a}_p^\dagger\hat{a}_q\hat{a}_p|\Psi(t_e)\rangle - \langle\Psi(t_e)|\hat{a}_q^\dagger\hat{a}_q|\Psi(t_e)\rangle\langle\Psi(t_e)|\hat{a}_p^\dagger\hat{a}_p|\Psi(t_e)\rangle, \quad (8)$$

which corresponds to the excess coincidence rate in a Hanbury Brown-Twiss-type measurement [64]. Positive values ($C_{qp} > 0$) indicate intermode photon bunching, negative values ($C_{qp} < 0$) indicate antibunching, and $C_{qp} = 0$ corresponds to uncorrelated modes.

Figure 3 shows the cross-correlation distributions under coherent and BSV driving. Consistent with single-mode statistics, correlations under coherent light are roughly five orders of magnitude smaller than under BSV light, indicating

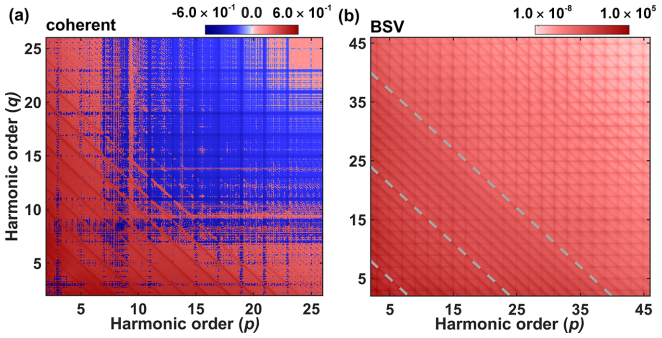

FIG. 3. Cross-correlation C_{qp} between harmonic modes (q, p) for (a) coherent light and (b) BSV light. Positive (negative) values indicate photon bunching (antibunching). The dashed lines (at $q + p = 10, 26, 42$) mark examples of antidiagonal stripe pattern.

that harmonic modes driven by coherent light are largely independent, whereas BSV driving produces strong intermode correlations. Even under coherent light, weak correlations reveal both positive and negative intermode behavior, with some mode pairs exhibiting bunching and others antibunching. Under BSV light, correlations are predominantly positive, reflecting the bunched nature of BSV and resulting in strong intermode photon bunching. Notably, antidiagonal correlation stripes tilted at 45° emerge, indicating enhanced intermode bunching when $q + p$ is even (examples are indicated by the dashed lines at $q + p = 10, 26, 42$).

IV. DISCUSSIONS

A. Comparison with Husimi-distribution-based methods

We compare the intermode correlations and harmonic spectra predicted by the fully quantum theory with those obtained from Husimi-distribution-based methods.

1. Brief overview of Husimi-distribution-based methods

We first recall the construction of Husimi-distribution-based methods, since the correlation and spectral observables compared below are evaluated using the resulting density matrix. At the initial moment $t = 0$, the density matrix of the system can be expressed as $\hat{\rho}(0) = \hat{\rho}_{\rm A}(0) \otimes \hat{\rho}_{\rm F}(0)$, with $\hat{\rho}_{\rm A}(0) = |g\rangle\langle g|$ being the atomic ground state and $\hat{\rho}_{\rm F}(0)$ being the initial state of the light field. Using the relation between the generalized Glauber P distribution and the Husimi Q distribution, $P(\alpha, \gamma^*) = \frac{1}{4\pi} \exp[-|\alpha - \gamma^*|^2/4] Q[(\alpha + \gamma^*)/2]$, the field density matrix can be represented as [28,54]

$$\hat{\rho}_{\rm F}(0) = \int d^2\alpha_l d^2\gamma_l \, \frac{1}{4\pi} \exp\left(-\frac{|\alpha_l - \gamma_l^*|^2}{4}\right) \times Q\left(\frac{\alpha_l + \gamma_l^*}{2}\right) \frac{|\alpha_l\rangle\langle\gamma_l^*|}{\langle\gamma_l^*|\alpha_l\rangle} \otimes_{q\neq l} |0_q\rangle\langle 0_q|, \quad (9)$$

where $|\alpha_l\rangle$ ($|\gamma_l\rangle$) denotes the coherent state of mode l with parameter α_l (γ_l).

The electric-field amplitude E_{α_l} and coherent parameter α_l are related by $E_{\alpha_l} = 2\epsilon_l^{(1)}\alpha_l$. Substituting this relation into the exponential factor in Eq. (9) gives, in the free-space limit $\epsilon_l^{(1)} \to 0$ (equivalently $V \to \infty$), $\lim_{\epsilon_l^{(1)}\to 0}(4\pi)^{-1}(4|\epsilon_l^{(1)}|^2)^{-1} \exp[-|E_{\alpha_l} - E_{\gamma_l}|^2/(16|\epsilon_l^{(1)}|^2)] = \delta^2(E_{\alpha_l} - E_{\gamma_l})$, with E_{α_l} held fixed [29,30]. Thus, Eq. (9) reduces approximately to

$$\hat{\rho}_{\rm F}(0) \approx \int d^2\alpha_l \, Q(\alpha_l) |\alpha_l\rangle\langle\alpha_l| \otimes_{q\neq l} |0_q\rangle\langle 0_q|, \quad (10)$$

and the initial density matrix of the full system is written as $\hat{\rho}(0) = \int d^2\alpha_l \, Q(\alpha_l) |\alpha_l\rangle\langle\alpha_l| \otimes_{q\neq l} |0_q\rangle\langle 0_q| \otimes |g\rangle\langle g|$.

For each diagonal coherent-state component, the electronic wavefunction is propagated under the classical field $\boldsymbol{E}_{\alpha_l}(t) = \langle\alpha_l|\hat{\boldsymbol{E}}_l(t)|\alpha_l\rangle$, satisfying $i\partial_t|\phi_{\alpha_l}(t)\rangle = [\hat{H}_{\rm A} + \hat{d}\cdot\boldsymbol{E}_{\alpha_l}(t)]|\phi_{\alpha_l}(t)\rangle$ [29,30,50]. The radiation field is then obtained from the harmonic response of the atom, $\gamma_k^{\alpha_l} \approx d_{\alpha_l}(\omega_k)$, where $d_{\alpha_l}(\omega_k) = \int_0^\infty d\tau e^{i\omega_k\tau}\langle\phi_{\alpha_l}(\tau)|\hat{d}|\phi_{\alpha_l}(\tau)\rangle$ is the Fourier transform of the semiclassical dipole driven by the classical field $\boldsymbol{E}_{\alpha_l}(t)$. Accordingly, the approximate system density matrix at time t is

$$\hat{\rho}(t) = \int d^2\alpha_l \, Q(\alpha_l) \left|\phi_{\alpha_l}(t)\right\rangle\left\langle\phi_{\alpha_l}(t)\right| \otimes |\alpha_l\rangle\langle\alpha_l| \otimes_{q\neq l} \left|\gamma_q^{\alpha_l}\right\rangle\left\langle\gamma_q^{\alpha_l}\right|. \quad (11)$$

This density matrix is then used to evaluate the cross-correlation function and HHG spectra within this framework.

2. Correlation signatures

The characteristic antidiagonal stripe patterns in Fig. 3(b) can be traced to the dipole correlation function derived from the fully quantum treatment, expressed as $C_{qp} \propto \sum_{\xi,n} |\langle\xi, n|\hat{\mathcal{M}}(t_e, \omega_q, \omega_p)|g, \phi_l\rangle|^2$. Since the harmonics generated by the quantum driving field are of odd order, the dipole operator can be approximated as $\hat{d}_{\rm I}(t) \equiv \sum_{h\in{\rm odd}} \hat{d}_{\rm I}(h\omega_l)e^{-ih\omega_l t}$. Substituting this form into the operator $\hat{\mathcal{M}}(t_e, \omega_q, \omega_p)$, we obtain

$$\langle\xi, n|\hat{\mathcal{M}}(t_e, \omega_q, \omega_p)|g, \phi_l\rangle \propto \left[\mathrm{sinc}\left(\frac{A_s + B_h}{2}t_e\right)e^{i\frac{A_s+B_h}{2}t_e} - \mathrm{sinc}\left(\frac{A_s}{2}t_e\right)e^{i\frac{A_s}{2}t_e}\right]\frac{t_e}{B_h}, \quad (12)$$

where $A_s = \omega_q - s\omega_l$ and $B_h = \omega_p - h\omega_l$, with $h, s \in$ odd. Because of the sinc function, pronounced tilted stripes in C_{qp} appear at conditions satisfying $A_s + B_h = 0$, corresponding to even values of $q + p$.

For comparison, applying the definition $C_{qp} = {\rm Tr}[\hat{\rho}(t_e)\hat{a}_q^\dagger\hat{a}_p^\dagger\hat{a}_q\hat{a}_p] - {\rm Tr}[\hat{\rho}(t_e)\hat{a}_q^\dagger\hat{a}_q]{\rm Tr}[\hat{\rho}(t_e)\hat{a}_p^\dagger\hat{a}_p]$ to the Husimi-distribution-based density matrix obtained in Eq. (11) gives

$$C_{qp}^{\rm Husimi} = \int d^2\alpha_l \, Q(\alpha_l)\left|d_{\alpha_l}(\omega_q)\right|^2\left|d_{\alpha_l}(\omega_p)\right|^2 - \left(\int d^2\alpha_l \, Q(\alpha_l)\left|d_{\alpha_l}(\omega_q)\right|^2\right) \times \left(\int d^2\alpha_l \, Q(\alpha_l)\left|d_{\alpha_l}(\omega_p)\right|^2\right). \quad (13)$$

These distinctive stripe features therefore cannot be reproduced by Eq. (13), which effectively treats the harmonic

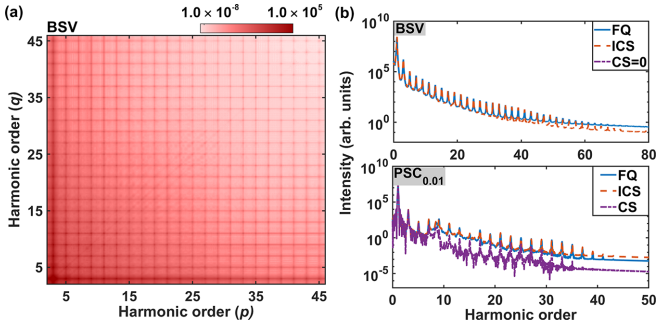

FIG. 4. (a) Cross-correlation C_{qp} between harmonic modes (q, p) for BSV light calculated via Husimi-distribution-based methods. (b) Comparison of the HHG spectra obtained from the FQ theory and Husimi-distribution-based methods for BSV light and PSC light with $\chi = 0.01$, where ICS and CS denote incoherent summation and coherent summation of semiclassical spectra, respectively.

modes of quantum light as classical probabilistic mixtures, as shown in Fig. 4(a). Moreover, when the driving field is coherent light, $Q(\alpha_l) = \delta(\alpha_l - \bar{\alpha}_l)$, Eq. (13) gives $C_{qp}^{\text{Husimi}} = 0$ because these methods treat harmonics as a multimode coherent state without intermode correlations. This sharply contrasts with the FQ theory [Fig. 3(a)], which preserves all coherence of the driving field and predicts weak positive and negative correlations for coherent states, entirely missed by Husimi-distribution-based methods.

3. High-harmonic spectra

The two-time correlation function shows that the HHG signal driven by quantum light contains two distinct contributions: the dipole expectation term and the dipole fluctuation term, as indicated in Eq. (5). Consequently, the HHG spectrum obtained within the fully quantum framework is derived self-consistently from first principles.

In contrast, methods based on the Husimi distribution can produce different spectra depending on how the summation over field states in Eq. (11) is performed—namely, through incoherent summation (ICS) or coherent summation (CS). For ICS, the harmonic yield in mode q is given by

$$Y_{\text{ICS}}(\omega_q) = \text{Tr}[\hat{\rho}(t_e)\hat{a}_q^\dagger \hat{a}_q] = \int d^2\alpha_l \, Q(\alpha_l)|d_{\alpha_l}(\omega_q)|^2. \quad (14)$$

For CS, the harmonic yield takes the form

$$Y_{\text{CS}}(\omega_q) = \left| \int_0^{t_e} d\tau \, e^{i\omega_q \tau} \text{Tr}[\hat{\rho}(\tau)\hat{d}] \right|^2 = \left| \int d^2\alpha_l \, Q(\alpha_l) d_{\alpha_l}(\omega_q) \right|^2. \quad (15)$$

This ambiguity originates from extending the semiclassical prescription for calculating HHG spectra—namely, taking the Fourier transform of the laser-driven atomic dipole while implicitly excluding the radiation-field Hilbert space—to the case of quantum driving fields. In strong-field processes driven by classical coherent light, this approach has been widely adopted and successfully reproduces experimental HHG spectra. However, the two expressions in Eqs. (14) and (15) are generally not equivalent. They become identical only in the coherent-state limit, where $Q(\alpha_l) = \delta(\alpha_l - \bar{\alpha}_l)$. As shown in Fig. 4(b), CS and ICS yield substantially different results: Even for PSC light with weak squeezing, CS predicts pronounced spectral suppression relative to ICS. Furthermore, CS cannot be applied to BSV light because the dipole contribution vanishes under coherent summation.

The comparison above demonstrates two important points. First, the ICS approach is in closer agreement with the fully quantum treatment than the CS approach. Second, although ICS reproduces the high-harmonic spectrum reasonably well, it fails to capture the essential correlation properties encoded in the photon statistics.

B. Origin of the differences

The differences discussed above can be traced to the sequence of approximations underlying Husimi-distribution-based approaches [29,30].

First, the quantum state of the driving field is expanded in the coherent-state basis through the generalized Glauber P representation, as expressed in Eq. (9). This transformation is formally exact and introduces no approximation.

Second, in the free-space limit, the off-diagonal components of the distribution are neglected because each individual contribution becomes exponentially suppressed. This approximation leads to Eq. (10), where only diagonal coherent-state components weighted by the Husimi distribution $Q(\alpha_l)$ are retained. Since the off-diagonal terms encode the quantum coherence of the driving field, their omission effectively converts the field into a diagonal statistical mixture. Furthermore, while each discarded off-diagonal contribution is individually small, the collective effect of the infinitely many neglected terms is not explicitly evaluated within this diagonal approximation. In practical implementations, the free-space limit is often employed further to simplify the original two-dimensional integral over coherent-state parameters into a one-dimensional integral over an effective field amplitude [29,30].

Third, the strong-field response associated with each diagonal coherent-state component is evaluated by retaining only its classical-field contribution. In this treatment, each coherent-state component acts effectively as a classical driving field, while the corresponding quantum corrections are assumed to be small and are therefore omitted. Their cumulative contribution over the full distribution is consequently neglected. Moreover, for each diagonal component, the emitted radiation modes are assumed to remain in coherent states, such that the total radiation field is represented as a tensor product of single-mode coherent states, and atom-field entanglement within that component is not explicitly retained. Together, these assumptions lead to the approximate density matrix given in Eq. (11).

Fourth, the results obtained from these classical-field calculations are recombined according to the diagonal distribution derived in the second step. For HHG, however, this final recombination introduces an ambiguity in the construction of the spectrum, leading to the ICS expression in Eq. (14) and the CS expression in Eq. (15).

Taken together, this sequence of approximations provides a practical framework for describing HHG driven by quantum light and effectively reduces the problem to averaging classical strong-field dynamics over intensity fluctuations. At the same time, it clarifies the origin of the discrepancies relative to the fully quantum treatment discussed above. In this sense, the fully quantum theory provides a first-principles benchmark for assessing the range of validity of these approximations and for identifying genuinely quantum features that remain inaccessible within such approximate descriptions [38].

C. The semiclassical limit

The fully quantum expression in Eq. (5) reduces to the semiclassical description of HHG when the quantum driving-field operator $\hat{\boldsymbol{E}}(t)$ is replaced by a classical field $\boldsymbol{E}_{\rm cl}(t)$, corresponding to the usual strong-field treatment of coherent-state driving in which field fluctuations are neglected. In this case, the dipole operator in the time domain is $\hat{d}_{\rm I}^{\rm sc}(t) = \hat{T}e^{i\int_0^t dt_1[\hat{H}_{\rm A}-\hat{d}\cdot\boldsymbol{E}_{\rm cl}(t_1)]}\hat{d}\hat{T}e^{-i\int_0^t dt_1[\hat{H}_{\rm A}-\hat{d}\cdot\boldsymbol{E}_{\rm cl}(t_1)]}$, and in the frequency domain $\hat{d}_{\rm I}^{\rm sc}(\omega) \equiv \int_0^{t_e} dt\hat{d}_{\rm I}^{\rm sc}(t)e^{i\omega t}$. The harmonic yield then takes the form

$$\begin{aligned} Y^{\rm sc}(\omega) &= \left|\langle g|\hat{d}_{\rm I}^{\rm sc}(\omega)|g\rangle\right|^2 + \langle g|\hat{d}_{\rm I}^{\rm sc}(\omega)|g\rangle^*\langle g|\Delta\hat{d}_{\rm I}^{\rm sc}(\omega)|g\rangle \\ &\quad + \langle g|\hat{d}_{\rm I}^{\rm sc}(\omega)|g\rangle\langle g|\Delta\hat{d}_{\rm I}^{\rm sc}(\omega)|g\rangle^* + \left|\langle g|\Delta\hat{d}_{\rm I}^{\rm sc}(\omega)|g\rangle\right|^2 \\ &= \left|\langle g|\hat{d}_{\rm I}^{\rm sc}(\omega)|g\rangle\right|^2, \end{aligned} \tag{16}$$

where, for simplicity, only the contributions in which the electron recombines to the ground state are included. The above derivation has used the property $\langle g|\Delta\hat{d}_{\rm I}^{\rm sc}(\omega)|g\rangle = 0$. This limit shows that the present formulation is self-consistent and contains the conventional HHG description as a special case.

D. Numerical convergence

Our calculation explicitly incorporates the degrees of freedom of the driving field. For strong fields, the associated Hilbert space can become extremely large. As discussed in Sec. II, the driving-field intensity is $I = \varepsilon_0 c|E|^2/2$ with the effective electric field amplitude $|E| = 2\epsilon^{(1)}\sqrt{N} = \sqrt{2\omega_l N/\epsilon_0 V}$. Therefore, the numerical results depend primarily on the ratio N/V instead of the absolute photon number N. We find that the numerical results converge rapidly as N increases while N/V is held fixed, as shown in Fig. 5. In practice, a driving-field basis of about 10^4 states is sufficient to obtain a converged HHG spectrum. Similar strategies have been employed in related works [31,56–58].

The calculations are carried out on a two-dimensional Cartesian spatial grid. For the electronic coordinate, the simulation box extends from $x_{\rm min} = -100$ a.u. to $x_{\rm max} = 100$ a.u., with a grid spacing of $dx = 0.1$ a.u. The driving-field mode, with an average photon number of $n = 10^4$, is represented on a spatial domain spanning from $y_{\rm min} = -1190$ a.u. to $y_{\rm max} = 1190$ a.u., using a grid spacing of $dy = 0.03$ a.u. For a smaller average photon number of $n = 5 \times 10^3$, the box can be reduced to $y_{\rm min} = -640$ a.u. to $y_{\rm max} = 640$ a.u., with a grid spacing of $dy = 0.06$ a.u. The time evolution is performed with a time step of $dt = 0.02$ a.u. In addition, the number of basis vectors used to represent the driving-field mode—expanded in the Fock-state basis—depends on the specific quantum state of the field. For coherent states and $\rm ASC_{0.01}$, the required upper limit of basis vectors exceeds 1.3 times the average photon number; for $\rm PSC_{0.01}$, it exceeds twice the average photon number; and for BSV, it exceeds 12 times the average photon number.

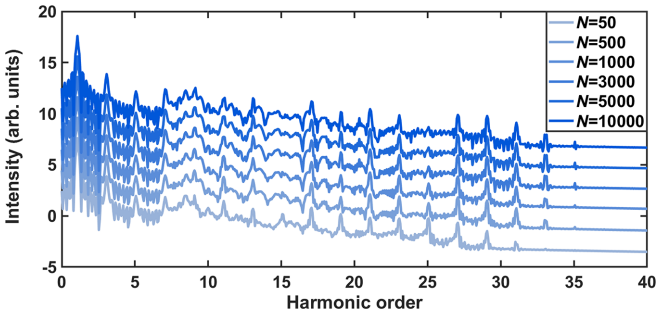

FIG. 5. Numerical convergence of HHG spectra for different average photon numbers N while keeping the effective field amplitude $|E| = \sqrt{2\omega_l N/\epsilon_0 V}$ fixed. Spectra are vertically offset for clarity.

E. Further remarks

Finally, we note that the interaction of intense quantum light with matter still raises many open questions. Our results suggest that HHG inherits key quantum properties of the driving field. This implies that for fields such as ASC, PSC, or even BSV, the emitted radiation should be revisited to determine whether the relative phases among different harmonic frequencies become more ordered or more irregular. Such studies are essential both for clarifying whether quantum-light-driven HHG can enable the generation of shorter attosecond pulses—or pulses with distinct quantum characteristics—and for achieving a proper characterization of the emitted radiation. Advancing these directions will be crucial for developing a comprehensive understanding of quantum HHG and promises to open new opportunities in ultrafast and quantum science.

V. CONCLUSION

We have developed a fully quantum, self-consistent theoretical framework for HHG driven by quantum light. Crucially, the theory shows that HHG persists even when the driving field has vanishing mean amplitude (e.g., BSV light), originating from correlations of dipole fluctuations rather than a nonzero dipole expectation value. The harmonic spectrum is thus directly linked to the dipole-correlation observable $\langle\hat{d}_{\rm I}(\omega)^\dagger\hat{d}_{\rm I}(\omega)\rangle$, providing a fundamental explanation of HHG under quantum driving fields.

Beyond reproducing HHG spectra across ASC, PSC, and BSV states, the framework reveals how the quantum statistics of the driving field are imprinted onto the harmonic modes. In particular, BSV light generates super-Poissonian statistics in individual harmonics and strong intermode photon bunching, opening new possibilities for engineering cross-frequency quantum correlations. More broadly, these results extend the understanding of quantum light-matter interactions, offering

predictive accuracy and analytical clarity that go beyond semiclassical approaches.

ACKNOWLEDGMENTS

We acknowledge helpful discussions with Professor Feng He. This work was supported by NSFC Grants No. U2330401, No. 12474484, No. 12088101, No. 12274384, and No. 12450404.

DATA AVAILABILITY

The data that support the findings of this article are openly available [65].

[1] A. McPherson, G. Gibson, H. Jara, U. Johann, T. S. Luk, I. McIntyre, K. Boyer, and C. K. Rhodes, Studies of multiphoton production of vacuum-ultraviolet radiation in the rare gases, J. Opt. Soc. Am. B **4**, 595 (1987).

[2] M. Ferray, A. L'Huillier, X. F. Li, L. A. Lompre, G. Mainfray, and C. Manus, Multiple-harmonic conversion of 1064 nm radiation in rare gases, J. Phys. B: At. Mol. Opt. Phys. **21**, L31 (1988).

[3] S. Ghimire and D. A. Reis, High-harmonic generation from solids, Nat. Phys. **15**, 10 (2019).

[4] P. M. Paul, E. S. Toma, P. Breger, G. Mullot, F. Augé, P. Balcou, H. G. Muller, and P. Agostini, Observation of a train of attosecond pulses from high harmonic generation, Science **292**, 1689 (2001).

[5] M. Hentschel, R. Kienberger, Ch. Spielmann, G. A. Reider, N. Milosevic, T. Brabec, P. Corkum, U. Heinzmann, M. Drescher, and F. Krausz, Attosecond metrology, Nature (London) **414**, 509 (2001).

[6] M. Drescher, M. Hentschel, R. Kienberger, G. Tempea, C. Spielmann, G. A. Reider, P. B. Corkum, and F. Krausz, X-ray pulses approaching the attosecond frontier, Science **291**, 1923 (2001).

[7] C. Gohle, T. Udem, M. Herrmann, J. Rauschenberger, R. Holzwarth, H. A. Schuessler, F. Krausz, and T. W. Hänsch, A frequency comb in the extreme ultraviolet, Nature (London) **436**, 234 (2005).

[8] G. Sansone, E. Benedetti, F. Calegari, C. Vozzi, L. Avaldi, R. Flammini, L. Poletto, P. Villoresi, C. Altucci, R. Velotta, *et al.*, Isolated single-cycle attosecond pulses, Science **314**, 443 (2006).

[9] P. B. Corkum and F. Krausz, Attosecond science, Nat. Phys. **3**, 381 (2007).

[10] K. C. Kulander, K. J. Schafer, and J. L. Krause, Dynamics of short-pulse excitation, ionization and harmonic conversion, in *Super-Intense Laser-Atom Physics*, NATO ASI Series Vol. 316 (Springer, Boston, MA, 1993), p. 95.

[11] K. J. Schafer, B. Yang, L. F. DiMauro, and K. C. Kulander, Above threshold ionization beyond the high harmonic cutoff, Phys. Rev. Lett. **70**, 1599 (1993).

[12] P. B. Corkum, Plasma perspective on strong field multiphoton ionization, Phys. Rev. Lett. **71**, 1994 (1993).

[13] M. Lewenstein, P. Balcou, M. Y. Ivanov, A. L'Huillier, and P. B. Corkum, Theory of high-harmonic generation by low-frequency laser fields, Phys. Rev. A **49**, 2117 (1994).

[14] I. N. Agafonov, M. V. Chekhova, and G. Leuchs, Two-color bright squeezed vacuum, Phys. Rev. A **82**, 011801 (2010).

[15] T. S. Iskhakov, A. M. Pérez, K. Y. Spasibko, M. V. Chekhova, and G. Leuchs, Superbunched bright squeezed vacuum state, Opt. Lett. **37**, 1919 (2012).

[16] A. M. Pérez, T. S. Iskhakov, P. Sharapova, S. Lemieux, O. V. Tikhonova, M. V. Chekhova, and G. Leuchs, Bright squeezed-vacuum source with 1.1 spatial mode, Opt. Lett. **39**, 2403 (2014).

[17] M. A. Finger, T. S. Iskhakov, N. Y. Joly, M. V. Chekhova, and P. S. J. Russell, Raman-free, noble-gas-filled photonic-crystal fiber source for ultrafast, very bright twin-beam squeezed vacuum, Phys. Rev. Lett. **115**, 143602 (2015).

[18] K. Y. Spasibko, D. A. Kopylov, V. L. Krutyanskiy, T. V. Murzina, G. Leuchs, and M. V. Chekhova, Multiphoton effects enhanced due to ultrafast photon-number fluctuations, Phys. Rev. Lett. **119**, 223603 (2017).

[19] M. Manceau, K. Y. Spasibko, G. Leuchs, R. Filip, and M. V. Chekhova, Indefinite-mean Pareto photon distribution from amplified quantum noise, Phys. Rev. Lett. **123**, 123606 (2019).

[20] P. R. Sharapova, G. Frascella, M. Riabinin, A. M. Pérez, O. V. Tikhonova, S. Lemieux, R. W. Boyd, G. Leuchs, and M. V. Chekhova, Properties of bright squeezed vacuum at increasing brightness, Phys. Rev. Res. **2**, 013371 (2020).

[21] S. Panahiyan, C. S. Muñoz, M. V. Chekhova, and F. Schlawin, Nonlinear interferometry for quantum-enhanced measurements of multiphoton absorption, Phys. Rev. Lett. **130**, 203604 (2023).

[22] J. Heimerl, A. Mikhaylov, S. Meier, H. Höllerer, I. Kaminer, M. Chekhova, and P. Hommelhoff, Multiphoton electron emission with non-classical light, Nat. Phys. **20**, 945 (2024).

[23] A. Rasputnyi, Z. Chen, M. Birk, O. Cohen, I. Kaminer, M. Krüger, D. Seletskiy, M. Chekhova, and F. Tani, High harmonic generation by bright squeezed vacuum, Nat. Phys. **20**, 1960 (2024).

[24] S. Lemieux, S. A. Jalil, D. N. Purschke, N. Boroumand, T. Hammond, D. Villeneuve, A. Naumov, T. Brabec, and G. Vampa, Photon bunching in high-harmonic emission controlled by quantum light, Nat. Photonics **19**, 767 (2025).

[25] M. E. Tzur, C. Mor, N. Yaffe, M. Birk, A. Rasputnyi, O. Kneller, I. Nisim, I. Kaminer, M. Krüger, N. Dudovich, *et al.*, Measuring and controlling the birth of quantum attosecond pulses, arXiv:2502.09427.

[26] Y. Kano, A new phase-space distribution function in the statistical theory of the electromagnetic field, J. Math. Phys. **6**, 1913 (1965).

[27] M. Hillery, R. F. O'Connell, M. O. Scully, and E. P. Wigner, Distribution functions in physics: Fundamentals, Phys. Rep. **106**, 121 (1984).

[28] M. S. Kim, F. A. M. De Oliveira, and P. L. Knight, Properties of squeezed number states and squeezed thermal states, Phys. Rev. A **40**, 2494 (1989).

[29] M. E. Tzur, M. Birk, A. Gorlach, M. Krüger, I. Kaminer, and O. Cohen, Photon-statistics force in ultrafast electron dynamics, Nat. Photonics **17**, 501 (2023).

[30] A. Gorlach, M. E. Tzur, M. Birk, M. Krüger, N. Rivera, O. Cohen, and I. Kaminer, High-harmonic generation driven by quantum light, Nat. Phys. **19**, 1689 (2023).
[31] M. E. Tzur and O. Cohen, Motion of charged particles in bright squeezed vacuum, Light: Sci. Appl. **13**, 41 (2024).
[32] M. E. Tzur, M. Birk, A. Gorlach, I. Kaminer, M. Krüger, and O. Cohen, Generation of squeezed high-order harmonics, Phys. Rev. Res. **6**, 033079 (2024).
[33] J. Rivera-Dean, P. Stammer, M. Ciappina, and M. Lewenstein, Structured squeezed light allows for high-harmonic generation in classical forbidden geometries, Phys. Rev. Lett. **135**, 013801 (2025).
[34] S. Wang, X. Lai, and X. Liu, Attosecond pulse synthesis from high-order harmonic generation in intense squeezed light, Phys. Rev. A **112**, L011102 (2025).
[35] S. Wang and X. Lai, High-order above-threshold ionization of an atom in intense quantum light, Phys. Rev. A **108**, 063101 (2023).
[36] Y. Fang, F. X. Sun, Q. He, and Y. Liu, Strong-field ionization of hydrogen atoms with quantum light, Phys. Rev. Lett. **130**, 253201 (2023).
[37] H. Liu, H. Zhang, X. Wang, and J. Yuan, Atomic double ionization with quantum light, Phys. Rev. Lett. **134**, 123202 (2025).
[38] R. V. Gothelf, C. S. Lange, and L. B. Madsen, High-order harmonic generation in a crystal driven by quantum light, Phys. Rev. A **111**, 063105 (2025).
[39] R. J. Glauber, Optical coherence and photon statistics, in *Quantum Optics and Electronics*, edited by C. DeWitt, A. Blandin, and C. Cohen-Tannoudji (Gordon and Breach, New York, 1965), p. 63.
[40] M. O. Scully and W. E. Lamb, Jr., Quantum theory of an optical maser. II. Spectral profile, Phys. Rev. **166**, 246 (1968).
[41] P. L. Knight and P. W. Milonni, The Rabi frequency in optical spectra, Phys. Rep. **66**, 21 (1980).
[42] J. D. Cresser, Theory of the spectrum of the quantised light field, Phys. Rep. **94**, 47 (1983).
[43] J. Eberly and M. Fedorov, Spectrum of light scattered coherently or incoherently by a collection of atoms, Phys. Rev. A **45**, 4706 (1992).
[44] A. Di Piazza, K. Z. Hatsagortsyan, and C. H. Keitel, Quantum radiation reaction effects in multiphoton Compton scattering, Phys. Rev. Lett. **105**, 220403 (2010).
[45] S. Yi, N. D. Klimkin, G. G. Brown, O. Smirnova, S. Patchkovskii, I. Babushkin, and M. Ivanov, Generation of massively entangled bright states of light during harmonic generation in resonant media, Phys. Rev. X **15**, 011023 (2025).
[46] J. Javanainen, J. H. Eberly, and Q. Su, Numerical simulations of multiphoton ionization and above-threshold electron spectra, Phys. Rev. A **38**, 3430 (1988).
[47] A. Bogatskaya, E. Volkova, and A. Popov, Prospects of odd and even harmonic generation by an atom in a high-intensity laser field, Laser Phys. Lett. **14**, 055301 (2017).
[48] D. N. Yangaliev, V. P. Krainov, and O. I. Tolstikhin, Quantum theory of radiation by nonstationary systems with application to high-order harmonic generation, Phys. Rev. A **101**, 013410 (2020).
[49] F. Gauthey, C. H. Keitel, P. L. Knight, and A. Maquet, Role of initial coherence in the generation of harmonics and sidebands from a strongly driven two-level atom, Phys. Rev. A **52**, 525 (1995).
[50] A. Gorlach, O. Neufeld, N. Rivera, O. Cohen, and I. Kaminer, The quantum-optical nature of high harmonic generation, Nat. Commun. **11**, 4598 (2020).
[51] I. Gonoskov, N. Tsatrafyllis, I. Kominis, and P. Tzallas, Quantum optical signatures in strong-field laser physics: Infrared photon counting in high-order-harmonic generation, Sci. Rep. **6**, 32821 (2016).
[52] N. Tsatrafyllis, I. Kominis, I. Gonoskov, and P. Tzallas, High-order harmonics measured by the photon statistics of the infrared driving-field exiting the atomic medium, Nat. Commun. **8**, 15170 (2017).
[53] S. de-la-Pena, O. Neufeld, M. E. Tzur, O. Cohen, H. Appel, and A. Rubio, Quantum electrodynamics in high-harmonic generation: Multitrajectory Ehrenfest and exact quantum analysis, J. Chem. Theory Comput. **21**, 283 (2025).
[54] M. O. Scully and M. S. Zubairy, *Quantum Optics* (Cambridge University Press, Cambridge, England, 1997).
[55] H. J. Carmichael, *Statistical Methods in Quantum Optics 1: Master Equations and Fokker-Planck Equations* (Springer, Berlin, Heidelberg, 1999).
[56] N. Tsatrafyllis, S. Kühn, M. Dumergue, P. Foldi, S. Kahaly, E. Cormier, I. Gonoskov, B. Kiss, K. Varju, S. Varro, *et al.*, Quantum optical signatures in a strong laser pulse after interaction with semiconductors, Phys. Rev. Lett. **122**, 193602 (2019).
[57] J. Rivera-Dean, Role of short and long trajectories on the quantum-optical state after high-order harmonic generation, Phys. Rev. A **110**, 063704 (2024).
[58] Y.-B. Wang and X.-B. Bian, High-order harmonic generation in quantum light by a generalized von Neumann lattice method, Phys. Rev. A **111**, 043111 (2025).
[59] A. M. Fox, *Quantum Optics: An Introduction*, Oxford Master Series in Atomic, Optical, and Laser Physics Vol. 15 (Oxford University Press, Oxford, 2006).
[60] C. C. Gerry and J. H. Eberly, Dynamics of a Raman coupled model interacting with two quantized cavity fields, Phys. Rev. A **42**, 6805 (1990).
[61] C. T. Lee, Nonclassical photon statistics of two-mode squeezed states, Phys. Rev. A **42**, 1608 (1990).
[62] C. C. Gerry and H. Huang, Dynamics of a two-atom Raman coupled model interacting with two quantized cavity fields, Phys. Rev. A **45**, 8037 (1992).
[63] C. C. Gerry and P. L. Knight, *Introductory Quantum Optics*, 2nd ed. (Cambridge University Press, Cambridge, England, 2023).
[64] H. Paul, Interference between independent photons, Rev. Mod. Phys. **58**, 209 (1986).
[65] H. Liu, Theory of high harmonic generation with quantum light (v1), figshare, 2026, https://doi.org/10.6084/m9.figshare.32664744.